Kalman-variant estimators for state of charge in lithium-sulfur batteries

Propp, Karsten; Auger, Daniel J.; Fotouhi, Abbas; Longo, Stefano; Knap, Vaclav

Published in:
Journal of Power Sources

DOI (link to publication from Publisher):
10.1016/j.jpowsour.2016.12.087

Publication date:
2017

Document Version
Publisher's PDF, also known as Version of record

Journal of Power Sources 343 (2017) 254–267

Contents lists available at ScienceDirect

Journal of Power Sources

journal homepage: www.elsevier.com/locate/jpowsour

Kalman-variant estimators for state of charge in lithium-sulfur batteries

Karsten Propp, Daniel J. Auger*, Abbas Fotouhi, Stefano Longo, Vaclav Knap [1]

School of Aerospace, Transport and Manufacturing, Cranfield University College Road, Bedford, MK43 0AL, UK

HIGHLIGHTS

- Li-S batteries differ to Li-ion batteries, and require specific state of charge estimation.
- We discuss the limitations of standard SoC estimation methods with Li-S.
- A set of applicable state-of-charge estimators for Li-S batteries is developed.
- The extended Kalman Filter (KF), unscented KF and Particle filter are applied.
- The performance of the applied recursive Bayesian filters is evaluated.

ARTICLE INFO

Article history:
Received 21 September 2016
Received in revised form
21 December 2016
Accepted 22 December 2016
Available online 20 January 2017

Keywords:
Lithium sulfur battery
State of charge
Extended Kalman filter
Unscented Kalman filter
Particle filter

ABSTRACT

Lithium-sulfur batteries are now commercially available, offering high specific energy density, low production costs and high safety. However, there is no commercially-available battery management system for them, and there are no published methods for determining state of charge *in situ*. This paper describes a study to address this gap. The properties and behaviours of lithium-sulfur are briefly introduced, and the applicability of 'standard' lithium-ion state-of-charge estimation methods is explored. Open-circuit voltage methods and 'Coulomb counting' are found to have a poor fit for lithium-sulfur, and model-based methods, particularly recursive Bayesian filters, are identified as showing strong promise. Three recursive Bayesian filters are implemented: an extended Kalman filter (EKF), an unscented Kalman filter (UKF) and a particle filter (PF). These estimators are tested through practical experimentation, considering both a pulse-discharge test and a test based on the New European Driving Cycle (NEDC). Experimentation is carried out at a constant temperature, mirroring the environment expected in the authors' target automotive application. It is shown that the estimators, which are based on a relatively simple equivalent-circuit–network model, can deliver useful results. If the three estimators implemented, the unscented Kalman filter gives the most robust and accurate performance, with an acceptable computational effort.

1. Introduction

Compared to today's widespread lithium-ion (Li-ion) battery technologies, lithium-sulfur (Li-S) offers increased specific energy storage capability [1]. A greater battery capacity is often advantageous, particularly in applications such as electric vehicles, where it can mitigate consumer concerns about driving range. Li-S batteries also have significant benefits in terms of their wide operational temperature window and safety [2]. The fact that sulfur is abundant and environmentally friendly is also attractive for large-scale cost-driven consumer applications. Commercialization has been hindered by the limitations of early-stage Li-S technologies such as quick degradation and limited sulfur utilization [3]. In recent years, considerable effort has been put into the exploration of Li-S's inner cell mechanisms, resulting in enhanced understanding [4]. Commercial cells are now available from suppliers such as OXIS Energy [5] and Sion Power [6]. Although today's cells may not fulfil every aspect of high automotive demands, they do open the opportunity for practical application oriented research.

In order to use a battery in a practical application, it is necessary

* Corresponding author.
E-mail address: d.j.auger@cranfield.ac.uk (D.J. Auger).
[1] Permanent address: Department of Energy Technology, Aalborg University, Aalborg, Denmark.

http://dx.doi.org/10.1016/j.jpowsour.2016.12.087
0378-7753/

to have an appropriate battery management system (BMS). A key function of the BMS is determining the remaining usable capacity of the battery, i.e. estimation of the state of charge (SoC). This is important for many reasons: the more accurately SoC is known, the greater the proportion of a battery that can be potentially utilized without fear of overcharging and over-discharging; for consumers, it is often helpful to know how much battery life remains.

In the automotive sector in particular, there has been much research on accurate and robust SoC estimation techniques for Li-ion batteries, aimed at meeting the demanding requirements of the automotive traction battery. Here, the batteries operate in an environment with varying power loads, different operation temperatures, noisy and crude measurements, and high safety requirements [7]. For systems with limited computational power, the SoC of a Li-ion battery can be estimated through the use of equivalent–circuit-networks (ECNs) [8,9], which simulate the voltage response of the battery. Due to their simplicity they are not able to give any insight into the inner cell reactions. However, in practice this does not matter: when operated within their specified limits—in terms of state-of-charge, temperature and current rates—performance of intercalation-based lithium-ion batteries is consistent and predictable [10–13]. This behaviour and the fact that the nonlinear relationship between open-circuit voltage (OCV) and SoC is monotonic means that it is relatively straightforward to determine a Li-ion battery's SoC [14].

For Li-ion batteries, there are many viable techniques for estimating SoC *in situ*. The simplest is to measure the open-circuit voltage and relate it through a nonlinear function or lookup table to the SoC. However, this method needs the battery to be in resting condition which limits the applicability for electric vehicles while driving. For improved robustness, OCV-based estimation is combined with other methods [15]. For a given value of SoC, ECN models can be used to predict terminal voltage output from a known dynamically-changing input current. This can be used to estimate SoC with a good compromise between accuracy, robustness and simplicity. A powerful approach is the use of 'observers' or 'state estimators' which combine model-based estimation with actual measurements using principles derived from control theory, particularly the Kalman filter and its derivatives. Estimators of this kind are popular (particularly within the automotive environment) due to their ability to handle measurement noise and model inaccuracies [7]. With these estimation methods, a high battery utilization is possible, without compromising battery safety or lifetime [16].

To date, estimation techniques of this kind have not been applied to Li-S batteries. There are big differences between Li-S and the classic Li-ion chemistry. Li-ion has an intercalation based process that has a single well-known dominant reaction pathway. Li-S batteries however are more complex with multiple pathways [17], which leads to some unusual and challenging behaviour for the SoC estimation: (i) the OCV-SoC curve has two voltage 'plateaus' with different properties; (ii) the OCV-SoC curve has a large flat region, where the OCV does not change with SoC; (iii) the batteries exhibit relatively high self discharge; and (iv) the usable capacity and power exhibit sensitivity to the applied current profile. Until recently, there have been no models of a Li-S cell suitable for use in a battery management algorithm. Recent developments have been made, and there are now published ECN models of Li-S batteries during discharge that are valid for a range of temperatures [18]. However, the use of these models for the estimation of SoC, remains unexplored. As initial step towards a full BMS system for Li-S batteries, this study examines SoC estimation techniques for their applicability to Li-S batteries.

In this paper, Sec. 2 introduces Li-S batteries and their properties. Sec. 3 explores the applicability of state-estimation techniques used for lithium-ion, noting the limitations with OCV measurement and 'Coulomb counting' and concluding that a more sophisticated approach is required. Sec. 4 describes the filtering techniques that will be used for estimation: Sec. 4.1 describes an equivalent circuit model that will be used to implement such filters, and Sec. 4.2–4.4 introduces three such filters: the extended (nonlinear) Kalman filter (EKF), the 'unscented' Kalman filter (UKF) and the particle filter (PF). Sec. 5 describes the experimental evaluation of these. The results are presented in Sec. 6 where their performance and applicability are discussed.

This work has been conducted as part of an automotive battery project, and the batteries used in this study are kept at a well-maintained constant temperature environment. Accordingly, the work in this paper has been restricted to a constant temperature. (In future work, this could be extended to a varying temperature environment.)

The key contribution of this paper is the development and analysis of these three recursive Bayesian SoC estimators for Li-S. To the best of the authors' knowledge, no similar work has appeared elsewhere in the literature.

2. Lithium-sulfur batteries

A Li-S battery consists of a lithium metal anode and a sulfur-based cathode in electrolyte. Sulfur reversibly reacts with lithium ions when reduced from elemental state S_8, via the intermediates $Li_2S_8, Li_2S_4, Li_2S_2$, to lithium sulfide Li_2S, which is the key of the high theoretical capacity of sulfur (1672 mAh g-1) [19]. The large number of different species however, lead to complex inner reactions that are still a matter of ongoing research [17]. As shown in Fig. 1, the discharge curve consists of two sections [20]: a high plateau at about 2.35 V OCV, characterized by the presence of a majority of high order polysulfides in solution (Li_2S_8, Li_2S_6), and a low plateau at around 2.15 V OCV, where lower order chains have been identified (Li_2S_4, Li_2S_3) [21].

In Li-S batteries the availability of these species in the electrolyte determine the battery's behaviour. In simple words, the cathode is dissolving and participating in electrolyte [22], which causes two voltage plateaus with different behaviour (usable capacity, internal resistance, self-discharge, transient behaviour) [23,24]. As an initial step to model these effects, an equivalent circuit model was presented recently, employing the Thevenin model structure with a pulse discharge current profile and an off-line prediction error minimisation method for parameter identification [18]. The model does not explicitly consider self-discharge, but is valid for transient behaviour of the kind seen in this study. In practice, lithium-sulfur batteries do experience significant self-discharge during long

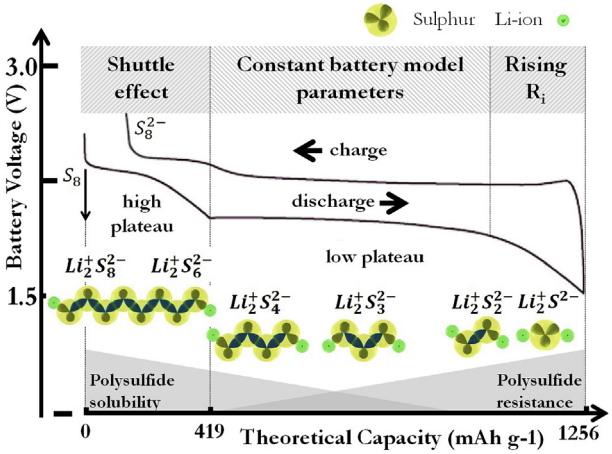

Fig. 1. Discharge/charge behaviour of a Li-S battery.

resting periods. For a shorter-term transient state estimation problem, this can be treated as uncertainty regarding the initial state. For details regarding the model derivation the reader is guided there.

Due to these unique properties of Li-S batteries, a precisely known SoC is helpful to predict the power capabilities of the battery, especially towards the end of discharge where the internal resistance raises quickly. It is not just near depletion that SoC estimation is important. Li-S batteries also need careful monitoring when they are close to fully charged to avoid the problem of 'shuttle'. While charging, the high solubility of the formed high-order polysulfide chains enables them to diffuse to the anode, where they can be reduced to lower order chains directly when in contact. The reaction circle is closed by the movement of the lower order chains back to the cathode. Here, they form high-order polysulfides again when the charging is continued. This redox reaction occurs without electrons passing through the external circuit of the battery and is called polysulfide shuttle [25], which leads, next to self-discharge in the high plateau, to poor coulombic efficiency and is associated with capacity fade [26]. Therefore overcharging should be avoided despite the fact that the shuttle effect can also protect the battery from being overcharged [19].

3. Applicability of conventional SoC estimation techniques

The behaviour of Li-S batteries discussed above leads to difficulties for SoC estimation. Each method faces different challenges: in the following section, these are explained in more detail for the most common SoC estimation techniques. (Impedance spectroscopy is not mentioned further, since it is seldom implemented for practical SoC estimation [15].)

Coulomb counting: Determining the charge flow in and out of the battery is the most common technique for SOC estimation since it is easy to implement. With a given starting point SoC_0 and the rated capacity, it is fairly simple to calculate the SoC from

$$SoC = SoC_0 + \frac{1}{C_N}\int_{t0}^{t}(I_{batt} - I_{loss})d\tau. \quad (1)$$

where C_N is the rated capacity, I_{batt} the battery current and I_{loss} the current consumed by loss reactions [15]. While this method is seen generally as reliable, it demands high precision current sensors (to reduce the accumulation of measurement errors over time), known values for the charge/discharge efficiency, and a precisely known initial condition [27,28]. These drawbacks lead to issues with the unique properties of Li-S batteries. Firstly, the polysulfide shuttle effect [25], mainly present in the high plateau, enhances self-discharge, poor coulombic efficiency and capacity fade [25,26]. This leads to hard to determine values for the I_{loss} or efficiency factors in the calculation and changing initial conditions for an estimator [29]. Secondly, the amount of sulfur that can be reversibly utilized during a discharge is strongly affected by the current profile, age and temperature [30]. Generally high discharge capacity is only obtained at low currents. High currents can produce a resistive layer on the cathode, hindering the utilization of the underlying sulfur [20]. This effect hampers the determination of the rated capacity, reducing the practicability of the Coulomb counting method itself significantly.

Open circuit voltage: Another common method of SoC estimation is to assign the OCV to the SoC. This is usually used in applications with low and constant currents or long resting periods. This method works well with Li-ion batteries, since they provide generally a monotonic rising relationships between OCV and SoC [14]. For Li-S however, this method is not feasible due to the non-monotonic curve, changing the gradient between the high and low plateau, and the stable OCV within the low plateau (Fig. 1). Furthermore, the whole concept of OCV for Li-S batteries is not clear due to self-discharge and precipitation [22].

Soft computing techniques: Avoiding the need for building a mathematical battery model and linearisation, soft computing techniques have the ability to model a highly non-linear system by establishing a relationship between the input and output of a system (a 'black-box' model) from training data. This makes these techniques suitable for consideration for battery applications. Particularly for SoC estimation, soft computing techniques have been used in previous studies for NiMH and Li-ion batteries [31,32]. However, there is no record in the literature where these techniques are used for Li-S batteries. (In Ref. [33], the idea is briefly proposed. However, estimation results are not presented.)

Model-based approaches: For the SoC estimation in highly dynamic environments, model-based solutions with a combination of adaptive algorithms are used. Their principle is based on an off-line established model, predicting the terminal voltage of the cell during operation and an adaptive algorithm, using the error between prediction and measurement to adjust the states. As the computational power of common BMSs are limited, simplified equivalent electrical circuits are often used to reproduce the transient behaviour of a battery [34,35]. In combination with algorithms such as the extended Kalman filter [36–38], unscented Kalman filter [39–41] and particle filter [42–44] ECN models can help to estimate the batteries internal states with relatively low computational effort and simple measurements of current and terminal voltage. The main advantage of model based methods is that they combine the benefits of direct voltage measurements and 'Coulomb counting' through the use of equivalent-circuit-network models, providing a formal framework for integrating model-based predictions with real-world voltage measurements. This may make them suitable for the properties of the Li-S chemistry. The principle behind these estimation algorithms is described in the following section.

4. Implementation of state estimators

As outlined in Sec. 2 and Sec. 3, Li-S batteries have poorly understood internal dynamics, and state-of-the-art ECN models that cannot represent every aspect of the cell in detail. Methods that have been found to be robust against unmodeled dynamics in the environment are recursive filters [45], that treat the model states x and the observations y as stochastic variables with associated probability density functions [46]. For Gaussian distributions the Kalman filter (KF), minimizing the error variance between true and estimated state, is heavily applied in battery state estimation. In such estimates, the process state is first estimated from a mathematical representation of the system dynamics; this is then corrected with feedback from measurements. The continuous model, described in Sec. 4.1, is used in its discrete form for propagation of prediction- and update-step.

$$\begin{aligned} x_k &= Ax_{k-1} + Bu_{k-1} + w_{k-1} \\ y_k &= Cx_k + v_k \end{aligned} \quad (2)$$

The additional terms w_k and v_k are random variables —white, zero mean, with normal distributions—representing process and measurement noise respectively. These describe the uncertainty in each equation. Their values are determined with the process noise covariance matrix Q and measurement noise covariance matrix R, which are usually assumed to be constant and chosen by the user. Simply speaking, the determined values affect whether the Kalman filter emphasises its 'trust' on feedback from measurements or the *a priori* estimates from the system model. Larger values indicate higher uncertainty or less trust in general. Referring to [47], the

Kalman filter equations are:
Time update equations:

$$\widehat{x}_k^- = A\widehat{x}_{k-1}^+ + Bu_{k-1} \tag{3}$$

$$P_k^- = AP_{k-1}^+A^T + Q \tag{4}$$

Measurement update equations:

$$L_k = P_k^- C^T \left(CP_k^- C^T + R\right)^{-1} \tag{5}$$

$$\widehat{x}_k^+ = \widehat{x}_k^- + L_k\left(y_k - C\widehat{x}_k^-\right) \tag{6}$$

$$P_k^+ = (I - L_k C)P_k^- \tag{7}$$

The beauty of the filter is that it provides an efficient recursive mean, minimizing the mean of the squared error, by supporting past, present and future states, even when the precise nature of the modelled system is unknown [47]. For the state estimation of Li-S batteries the nonlinear derivatives of the KF [48] (EKF, UKF) and the particle filter (PF) are employed.

The following describes the mathematics of the three recursive filter algorithms that were implemented. All three algorithms used the same nonlinear equivalent-circuit–network model (Sec. 4.1); the three algorithms are the extended Kalman filter (Sec. 4.2), the unscented Kalman filter (Sec. 4.3) and the particle filter (Sec. 4.4).

4.1. Equivalent-circuit–network model

The Li-S battery model, used in this work, is developed and described in detail in Ref. [18] for temperatures from 20 °C to 50 °C. Here however, the temperature is assumed to be constant, assuming a controlled BMS environment at 20 °C. The identification for a Thevenin equivalent circuit model (Fig. 2) is done with a similar mixed current pulse discharge as shown in Fig. 3-A. The mixed pulse pattern in combination with identification for each pulse individually is used to unveil current-dependent parameter changes in the model. There is self-discharge in the battery, but it is only significant during long resting periods, so I_{self} can be neglected for transient applications. Fig. 2 shows the identification results, as well as the chosen simplified parameter functions over the SoC (X) for the modelled parameters. For the observer the identified parameters of all pulses are used to fit polynomial functions over SoC for the open circuit voltage U_{OCV}, the internal resistance R_0 and one parallel RC circuit C_p and R_p with MATLAB [49]. Then the derived functions are included in the general state-space form

$$\begin{aligned} \dot{x}(t) &= A(t)x(t) + B(t)u(t) \\ y(t) &= C(t)x(t) + D(t)u(t). \end{aligned} \tag{8}$$

The dynamic states $x = [x_1\ x_2]^T$ of the system are the voltage over the RC circuit U_p and the SoC (X), calculated through Coulomb counting. The corresponding state space representation gives

$$A = \begin{bmatrix} \dfrac{-1}{f_{R_p}(X)\, f_{C_p}(X)} & 0 \\ 0 & 0 \end{bmatrix} B = \begin{bmatrix} \dfrac{1}{f_{C_p}(X)} \\ \dfrac{-1}{3600 Q_{cap}} \end{bmatrix} \tag{9}$$

$$C = [-1 \quad f_{OCV}(X)]D = \left[f_{R_0}(X)\right].$$

In Ref. [18] it was shown that the current dependencies of the model parameters mostly influence the transient voltage behaviour, represented by C_p and R_p, and that they can be neglected without compromising the accuracy of the model significantly. But because of the parameter patterns of U_{OCV} and R_0 vary strongly between the high- and low plateau (Fig. 2), two separate polynomials were fitted over the SoC for each plateau respectively. (A single polynomial would be impractical, since behaviour changes significantly between the plateaus.)

The transition between the polynomials is realized smoothly and differentiably via a partial sinusoidal function $\gamma_{m,c}$.

$$\gamma_{m,c}(X) := \begin{cases} 0, & \text{if a} \\ \dfrac{1}{2} + \dfrac{1}{2}\sin(2m(X-c)), & \text{if b} \\ 1, & \text{if c} \end{cases} \tag{10}$$

where the conditions a, b, c stands for the different ranges of the function,

$$\begin{aligned} &\text{a}: \ 2m(X-c) < -\frac{1}{2}\pi, \\ &\text{b}: \ -\frac{1}{2}\pi \le 2m(X-c) < \frac{1}{2}\pi, \\ &\text{c}: \ 2m(X-c) > \frac{1}{2}\pi, \end{aligned} \tag{11}$$

where m is a scaling factor for the maximal gradient of the sinusoidal function, determining the transition range between both polynomials and c represents the point where both functions are equally represented. The combined equations of both polynomials and factor γ are

$$f_{OCV}(X) = \left(1 - \gamma_{m,c}(X)\right)\ f_{OCV-low}(X) + \gamma_{m,c}(X) f_{OCV-high}(X) \tag{12}$$

for the open circuit voltage U_{OCV} and

$$f_{R0}(X) = \left(1 - \gamma_{m,c}(X)\right)\ f_{R0-low}(X) + \gamma_{m,c}(X)\, f_{R0-high}(X), \tag{13}$$

for the internal resistance R_0 over SoC. Since the variations between both plateaus are less pronounced for C_p and R_p, the functions for these parameters are only determined with a single polynomial respectively. This decision also simplifies the estimation of the Jacobian matrix of A for the extended Kalman filter.

For a fuller discussion of this ECN model, the reader is referred to the original source [18].

4.2. Extended Kalman filter

The basic Kalman filter algorithm, described in Sec. 4, applies to linear systems, not nonlinear systems. The Li-S equivalent-circuit–network is *nonlinear*. This means that the basic algorithm needs adaptation before it can be applied. There are several ways of doing this, which will be explored in the following sections. The simplest is the 'extended Kalman filter' (EKF).

The basic idea of the EKF is to linearise the system around the current mean of the state $\widehat{x}_{k-1}^+$ with a first order Taylor series for the propagation of the probability densities [50]. Hence, the EKF predicts the states and measurements with a nonlinear system model f and the covariances and Kalman gain with the Jacobians of A and C, $\widehat{A}$ and $\widehat{C}$. Generally this linearisation works well with models containing slight non-linearities as it is the case for most classic Li-ion batteries.

Determining the Jacobians analytically increases the effort for

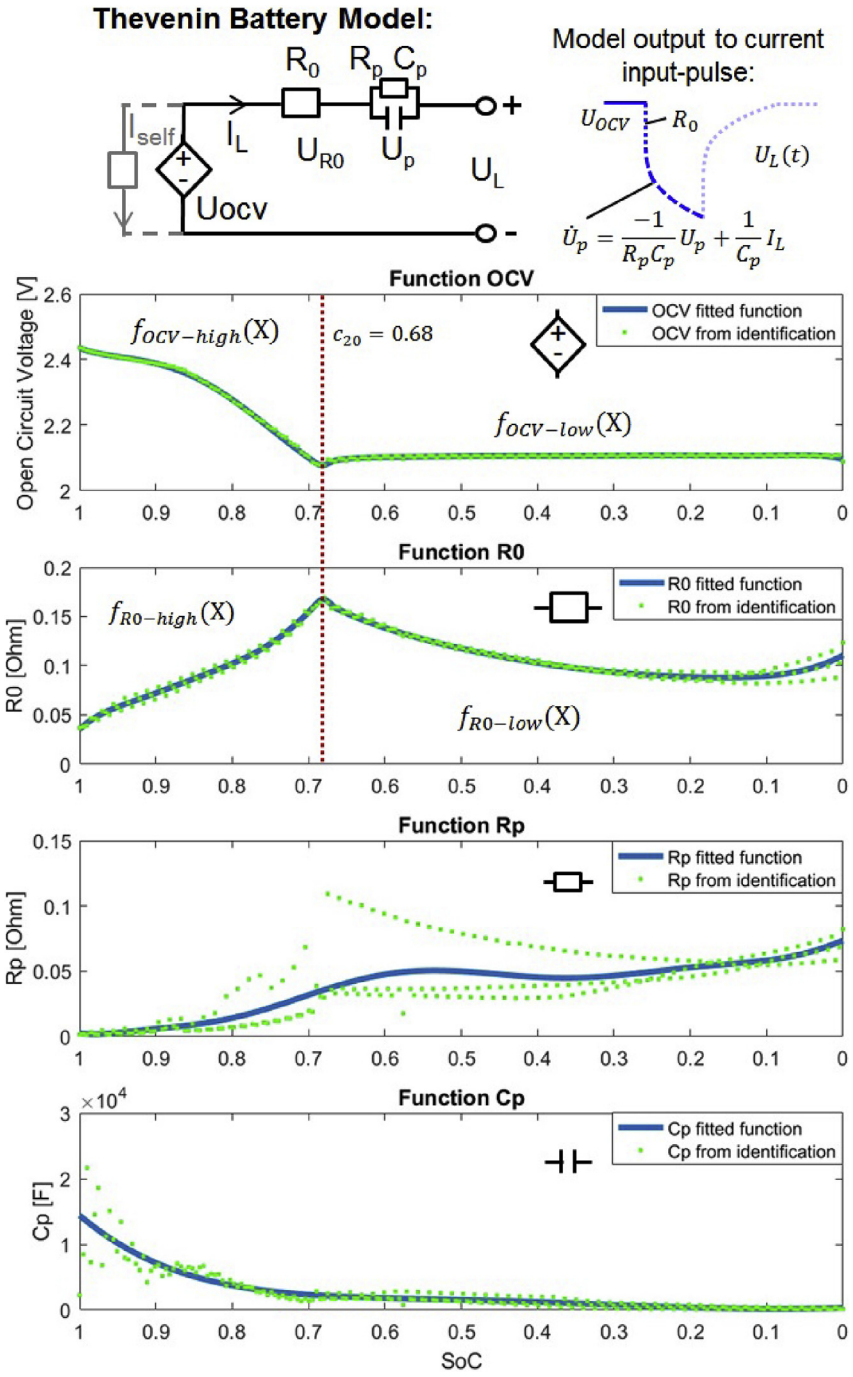

Fig. 2. Model structure and parameter functions for U_{OCV}, R_0, R_p and C_p over SoC for 20 °C.

setting up the filter with the benefit of the lowest computational effort of the proposed methods.

4.2.1. Summary of EKF algorithm

In the following, the algorithm is summarized from Ref. [16]. (Details are omitted here for brevity, but can be found in the reference.)

Nonlinear state space model

$$x_k = f(x_{k-1}, u_{k-1}, w_{k-1}, k-1)$$
$$y_k = h(x_k, u_k, v_k, k)$$

Definitions

$$\widehat{A}_k = \frac{\partial f(x_k, u_k, w_k, k)}{\partial x_k}\Big|_{x_k=\widehat{x}_k^+}, \widehat{B}_k = \frac{\partial f(x_k, u_k, w_k, k)}{\partial w_k}\Big|_{w_k=\overline{w}_k},$$
$$\widehat{C}_k = \frac{\partial h(x_k, u_k, w_k, k)}{\partial x_k}\Big|_{x_k=\widehat{x}_k^-}, \widehat{D}_k = \frac{\partial h(x_k, u_k, w_k, k)}{\partial v_k}\Big|_{v_k=\overline{v}_k}$$

Initialisation for k = 0

$$\widehat{x}_0^+ = \mathbb{E}[x_0],\ P_0^+ = \mathbb{E}\left[\left(x_0 - \widehat{x}_0^+\right)\left(x_0 - \widehat{x}_0^+\right)^T\right]$$

Computation EKF for k = 1, 2, …

State estimate update:

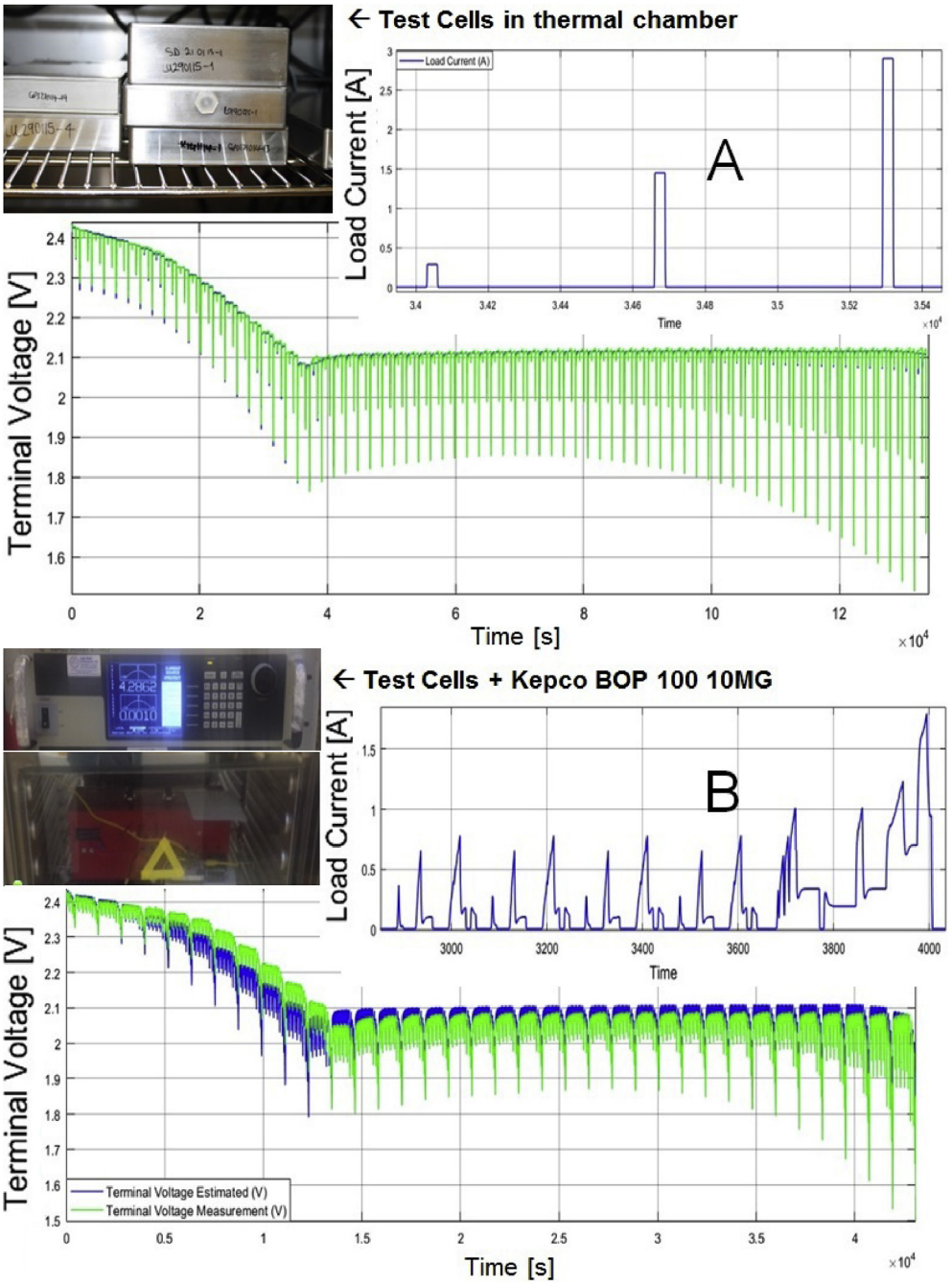

Fig. 3. Mixed pulse and NEDC current profile with test installation.

$$\widehat{x}_k^- = f\left(\widehat{x}_{k-1}^+, u_{k-1}, \overline{w}_{k-1}, k-1\right)$$

Error covariance update:

$$P_k^- = \widehat{A}_{k-1} P_{k-1}^+ \widehat{A}_{k-1}^T + \widehat{B}_{k-1} Q\, \widehat{B}_{k-1}^T$$

Output estimate:

$$\widehat{y}_k = h\left(\widehat{x}_k^-,\ u_k\ ,\ v_k, k\right)$$

Kalman Gainmatrix:

$$L_k = P_k^- \widehat{C}_k^T \left[\widehat{C}_k P_k^- \widehat{C}_k^T + \widehat{D}_k R_k \widehat{D}_k^T\right]^{-1}$$

State estimate measurement update:

$$\widehat{x}_k^+ = \widehat{x}_k^- + L_k[y_k - \widehat{y}_k]$$

Error covariance measurement update:

$$P_k^+ = (I - L_k \widehat{C}_k) P_k^-$$

4.3. Unscented Kalman filter

To improve the estimation for nonlinear systems, the covariance propagation in the UKF follows the nonlinearities with a set of sigma points, propagated through the main steps of the algorithm. The number of necessary points depends on the state vector's dimension L and leads to $2L + 1$ columns for the resulting vector χ. With the principle of estimating covariances with data rather than

a Taylor series, the unscented Kalman filter has the advantage that no derivatives are needed, with only slightly more computational effort. Furthermore, the covariance approximations are usually better than these of the EKF [16]. The differences between both are largely dependent on the nonlinearity of the system. For standard Li-ion batteries for example, the improvements are modest due to their small nonlinearities [16].

4.3.1. Summary of UKF algorithm

In the following the algorithm is summarized from Ref. [51]. (Again, details are omitted here for brevity, but can be found in the reference.)

Nonlinear state space model

$$x_k = f(x_{k-1}, u_{k-1}) + w_{k-1} \quad y_k = h(x_k, u_k) + v_k$$

Definitions

$$Q_k = \mathbb{E}\left[w_k w_k^T\right] \quad R_k = \mathbb{E}\left[v_k v_k^T\right]$$

Initialisation

$$\widehat{x}_0^+ = \mathrm{E}[x_0]$$

$$P_0^+ = \mathrm{E}\left[\left(x_0 - \widehat{x}_0^+\right)\left(x_0 - \widehat{x}_0^+\right)^T\right]$$

Computation UKF for k = 1, 2, …
State estimate time update

Errorcovariance matrix squareroot :

$$\sqrt{P_{k-1}} = \mathrm{chol}(P_{k-1})$$

Create sigma points:

$$\chi_{k-1}^+ = \left[\widehat{x}_{k-1}^+,\ \widehat{x}_{k-1}^+ + \gamma\sqrt{P_{k-1}^+},\ \widehat{x}_{k-1}^+ - \gamma\sqrt{P_{k-1}^+}\right]$$

Update sigma points:

$$\chi_k^{i,-} = f\left(\chi_{k-1}^{i,+}, u_{k-1}\right) \text{ for i } = 0, 1, 2 \ldots 2\mathrm{L}$$

Mean of updated sigma points:

$$\widehat{x}_k^- = \sum_{i=0}^{2L} \alpha_i^{(m)} \chi_k^{i,-}$$

Error Covariance time update
Covariance prediction:

$$P_k^- = Q_{k-1} + \sum_{i=0}^{2L} \alpha_i^{(c)} \left(\chi_k^{i,-} - \widehat{x}_k^-\right)\left(\chi_k^{i,-} - \widehat{x}_k^-\right)^T$$

Output estimate
Measurement prediction for each sigma point:

$$\psi_k^i = h\left(\chi_k^{i,-}, u_k\right) \text{ for i } = 0, 1, 2 \ldots 2\mathrm{L}$$

Mean of the measurement prediction:

$$\widehat{y}_k = \sum_{i=0}^{2L} \alpha_i^{(m)} \psi_k^i$$

Estimator gain matrix
Estimate the covariance of measurement:

$$P_k^{yy} = R_k + \sum_{i=0}^{2L} \alpha_i^{(c)} \left(\psi_k^i - \widehat{y}_k\right)\left(\psi_k^i - \widehat{y}_k\right)^T$$

Estimate cross covariance state/measurement:

$$P_k^{xy} = \sum_{i=0}^{2L} \alpha_i^{(c)} \left(\chi_k^{i,-} - \widehat{x}_k^-\right)\left(\psi_k^i - \widehat{y}_k\right)^T$$

Kalman gain:

$$L_k = P_k^{yy}\left(P_k^{xy}\right)^{-1}$$

State estimate update:

$$\widehat{x}_k^+ = \widehat{x}_k^- + L_k(y_k - \widehat{y}_k)$$

Error covariance update:

$$P_k^+ = P_k^- - L_k P_k^{yy} L_k^T$$

4.4. Particle filter

To solve the recursive estimation problem for arbitrary probability distributions, the PF applies Monte Carlo methods to represent the probability density functions. Unlike the UKF, where just the means and covariances of the sigma points are transferred to the next step, the PF recursively estimates the whole particle set χ_t from the last step χ_{t-1}. Generally three steps are executed [52]. (i) The state transition, where each particle transition is calculated with the input u_{k-1}, after measurement noise is added to the particles of the previous step. Similar to the Kalman filter, the addition of the noise leads to an increasing variance over time. (ii) In the weighting step the observations y_k and a probability density function are used to allocate a weight to each particle, representing the probability state prediction x_k given a certain observation y_k. (iii) During resampling, the variance of the particle set is decreased by sampling a new set of particles according to their weights and allocating new, equal weights. The main advantage of the PF is the independence of the Gaussian noise assumption of the Kalman filter. However, since each particle has to be computed separately, the computational effort exceeds the Kalman filter type algorithms significantly [53].

4.4.1. Summary of PF algorithm

The derivation of the equations orients on chapter 4.2 of the textbook [54]. (Again, details are omitted here for brevity, but can be found in the reference.)

$$\bar{\chi}_k = \chi_k = \varnothing$$

for $m = 1$ to M do

$$\text{sample } x_k^m \approx p(x_k | u_k, x_{k-1}^m)$$

$$w_k^m = p(y_k | x_k^m)$$

$$\bar{\chi}_k = \bar{\chi}_k + \langle x_k^m, w_k^m \rangle$$

endfor

for $m = 1$ to M do

$$\text{draw } i \text{ with probability} \propto w_k^i$$

$$\text{add } x_k^i \text{ to } \chi_k$$

endfor

return χ_k

5. Experimental evaluation

To investigate the performance of the state estimation algorithms, batteries were discharged with two current profiles and different test rigs. The first, a mixed-current pulse test, is based on the parameter estimation in Ref. [18] and represents an abstract test in a controlled environment. Here, a pre-cycled (C/10 charge, C/5 discharge, 30 °C) 3.4 Ah long life chemistry pouch cell from OXIS Energy was tested with current pulses of 290 mA, 1450 mA and 2900 mA at 20 °C (Fig. 3-A). The test hardware included a Maccor 4000 battery tester with cells constantly held at temperature in sealed aluminium boxes inside a Binder KB53 thermal chamber, also shown in Fig. 3-A.

To represent a more practical scenario, the same kind of OXIS Energy cell was discharged with a current profile based on the New European Driving Cycle (NEDC) [55]. The related power profile, shown in Ref. [56], was chosen due to its compromise of a realistic user scenario, also containing some level of abstraction. The test hardware used in this case is a Kepco BOP100-10MG programmable power source/sink (Fig. 3-B) discharging a battery at room temperature (23 °C). The details of the experiments are summarized in Table 1.

5.1. Reference SoC estimation

The reference SoC for both test benches was calculated from the cumulated current, operating in the cells' recommended voltage range, i.e. between 2.45 V (fully charged, SoC = 1), and 1.5 V (fully discharged, SoC = 0).

$$SoC = SoC_{(0)} - \frac{1}{3600 Q_{\text{cap}}} \int_0^t i(\tau) d\tau. \tag{14}$$

While Coulomb counting is a poor predictor during tests, the discharge capacity for a specified voltage window can be calculated retrospectively, giving a reference SoC that can be used for post-experimental interpretation.

5.1.1. EKF SoC estimation

For the application of the EKF algorithm with the presented Li-S battery model, the Jacobians of the matrices A and C are needed, which are presented here for convenience. With one polynomial function respectively for C_p and R_p dependent on the SoC (here presented as second state of the model x_2), the Jacobian matrix of A is populated as:

$$\widehat{A}(1,1) = \frac{-1}{f_{C_p}(x_2)\, f_{R_p}(x_2)} \quad \widehat{A}(2,1) = 0 \quad \widehat{A}(2,2) = 0 \tag{15}$$

$$\widehat{A}(1,2) = \left[\frac{\dot{f}_{C_p}(x_2)}{f_{C_p}(x_2)^2 f_{R_p}(x_2)} + \frac{\dot{f}_{R_p}(x_2)}{f_{C_p}(x_2) f_{R_p}(x_2)^2}\right] x_1 - \left[\frac{\dot{f}_{C_p}(x_2)}{f_{C_p}(x_2)^2}\right] I_{Bat}, \tag{16}$$

with the same principle for C

Table 1
Discharge experiments.

Discharge	Measured Cap.	Av. Power	Av. Temp.
Pulse	9778 As	0.147 W	20 °C
NEDC	9678 As	0.467 W	23 °C

$$\widehat{C}(1,1) = -1 \quad \widehat{C}(1,2) = \dot{f}_{OCV}(x_2) - \dot{f}_{R_0}(x_2) I_{\text{Bat}}. \tag{17}$$

The derivatives of the combined functions $\dot{f}_{\text{OCV}}$ and $\dot{f}_{R_0}$ with respect to x_2 are influenced by the introduced factor γ, here substituted by $f_\gamma(x_2)$.

$$f_{\text{OCV}}(x_2) = \Big(1 - f_\gamma(x_2)\Big) f_{\text{OCV-low}}(x_2) + f_\gamma(x_2) f_{\text{OCV-high}}(x_2) \tag{18}$$

Derivation with respect to x_2 leads to

$$\begin{aligned} \dot{f}_{\text{OCV}}(x_2) = \dot{f}_{\text{OCV-low}}(x_2) - \Big(&\dot{f}_\gamma(x_2) f_{\text{OCV-low}}(x_2) \\ &+ f_\gamma(x_2) \dot{f}_{\text{OCV-low}}(x_2)\Big) + \dot{f}_\gamma(x_2) f_{\text{OCV-high}}(x_2) \\ &+ f_\gamma(x_2) \dot{f}_{\text{OCV-high}}(x_2). \end{aligned} \tag{19}$$

where $\dot{f}_\gamma$ is defined by

$$\dot{\gamma}_{m,c}(x_2) := \begin{cases} 0, & \text{if a} \\ m\cos(2m(x_2 - c)), & \text{if b} \\ 0, & \text{if c} \end{cases} \tag{20}$$

with the same conditions for a, b, c as in equation (11). The derivation of $\dot{f}_{R_0}$ follows the same pattern. As mentioned before, the unique behaviour of the Li-S battery can vary in a complex manner. Therefore it is reasonable to assume that the voltage prediction of the observer is, firstly, not necessarily accurate and, secondly, that the predicted voltage is not everywhere an indicator of the SoC. To account for this, the measurement noise value R is with 0.15 relatively high compared to the chosen model noise Q, which assumes uncorrelated states with a low uncertainty for the Coulomb counting state.

$$P_{0\ \text{EKF}} = \begin{bmatrix} 10 & 0 \\ 0 & 10 \end{bmatrix} \quad Q_{\text{EKF}} = \begin{bmatrix} 0.1 & 0 \\ 0 & 0.0000003 \end{bmatrix} \tag{21}$$

The value of the measurement noise R implies a standard deviation for the measurements of 387 mV. This is greater than the values of actual Gaussian noise observed from the measurements. However, since the battery model is not able to predict the terminal voltage for every user case precisely, deviations in this order of magnitude are possible. The values of Q, representing the system noise, were determined iteratively to give good results.

5.1.2. UKF SoC estimation

Within the UKF framework, the weights $\alpha_i^{(m)}$ and $\alpha_i^{(c)}$ are vectors containing real constant scalars with the conditions that $\sum_{i=0}^{p} \alpha_i^{(m)}$ and $\sum_{i=0}^{p} \alpha_i^{(c)}$ are equal to 1 [16]. With the scaling value

$$\lambda = \alpha^2 (L + \kappa) - L$$

the weights can be calculated from

$$\gamma = \sqrt{L + \lambda}, \quad \alpha_i^{(m)} = \alpha_i^{(c)} = \frac{1}{2(L + \lambda)}$$

$$\alpha_0^{(m)} = \frac{\lambda}{L + \lambda}, \quad \alpha_0^{(c)} = \frac{\lambda}{L + \lambda} + \Big(1 - \alpha^2 + \beta\Big).$$

Here, we chose similar weights as presented in Ref. [51], defining the values 1 for α, 2 for β, $L = \dim\{x\} = 2$, and 0 for κ. Since the parameters are constant, they can be defined once prior executing the filter. The values of the measurement and system noise R and Q follow the same pattern of the EKF. However, the values for P_0 are considerably smaller since widely spread,

unrestricted sigma points lead to estimation errors when they exceed the defined SoC range of 0–1 in the beginning of the estimation. Furthermore, the UKF was found to be more sensitive to the model prediction errors compared to the EKF, so larger values were used in the measurement noise matrix $R = 0.3$.

$$P_{0\,\mathrm{UKF}} = \begin{bmatrix} 1 & 0 \\ 0 & 0.014 \end{bmatrix} \quad Q_{\mathrm{UKF}} = \begin{bmatrix} 0.0005 & 0 \\ 0 & 0.0000007 \end{bmatrix} \tag{22}$$

5.1.3. PF SoC estimation

The chosen probability density function should, on the one hand, accurately determine the most likely observations, but on the other hand hinder the impoverishment of the samples over time. Examples for non Gaussian probability density functions for SoC estimation are given in Refs. [43,44]. Here however, the Gaussian distribution

$$f(x) = \frac{1}{\sigma\sqrt{2\pi}} e^{-\frac{(x-\mu)^2}{2\sigma^2}} \tag{23}$$

is used due to its simplicity and comparably to the EKF and UKF. To account for the uncertainties of the model and Coulomb counting, the standard deviations to sample the states in the prediction step are chosen in the same pattern as the EKF and UKF, allocating larger values to the transient voltage term U_p, to account for the model inaccuracies, and smaller values to the SoC state, to limit the random fluctuations when the battery behaviour does not change.

$$\mathrm{std}_{x_1} = 0.004 \quad \mathrm{std}_{x_2} = 0.0003 \tag{24}$$

The number of particles was chosen iteratively. Tests indicated a decent compromise between computational effort and estimation precision with a constant number of 30 particles.

6. Results and discussion

The results of the proposed SoC estimation algorithms are evaluated qualitatively for their convergence time, with imprecise initial states, and quantitatively by their estimation accuracy. As measure for the latter the root mean squared error (RMSE) over the hole discharge range is used.

$$\mathrm{RMSE} = \frac{1}{\sqrt{n}} \left(\sum_{i=1}^{n} \left(SoC_{t,i} - \hat{SoC}_{t,i} \right)^2 \right)^{0.5} \tag{25}$$

where n is the number of data points, $SoC_{t,i}$ is the reference SoC from the measurement and $\hat{SoC}_{t,i}$ is the estimated SoC by the filters. The accuracy and convergence depend on the quality of the model, the observability of the system itself, the quality of the measurements, their noise pattern and the users choices for the system and measurement uncertainties. In the context of the model accuracy also the discharge profile plays a role. For the pulse test, with its long resting periods, the errors in the OCV are more sensitive to the prediction error, whereas the more realistic NEDC cycle emphasises the internal resistance or transient behaviour. Since Li-S batteries suffer from self-discharge, which can lead to an imprecise initial condition for the SoC estimation, each test is performed with three different initial SoC values. While two of them are located in the high plateau ($SoC_0 = 1,\ 0.7$), one is chosen after the transition point (0.68) at ($SoC_0 = 0.6$), to test the algorithms ability to converge in between both plateaus. To test their robustness against current profile induced changes, all filters use the predetermined capacity from the mixed pulse discharge profile tests during the model identification (9778 As). The results of the SoC estimation tests are shown in Fig. 4 and Table 2. The following discussion orients on the specific properties of Li-S batteries.

High self-discharge: Self discharge, caused by the shuttle effect, occurs mainly in the high plateau. This can be difficult to handle for

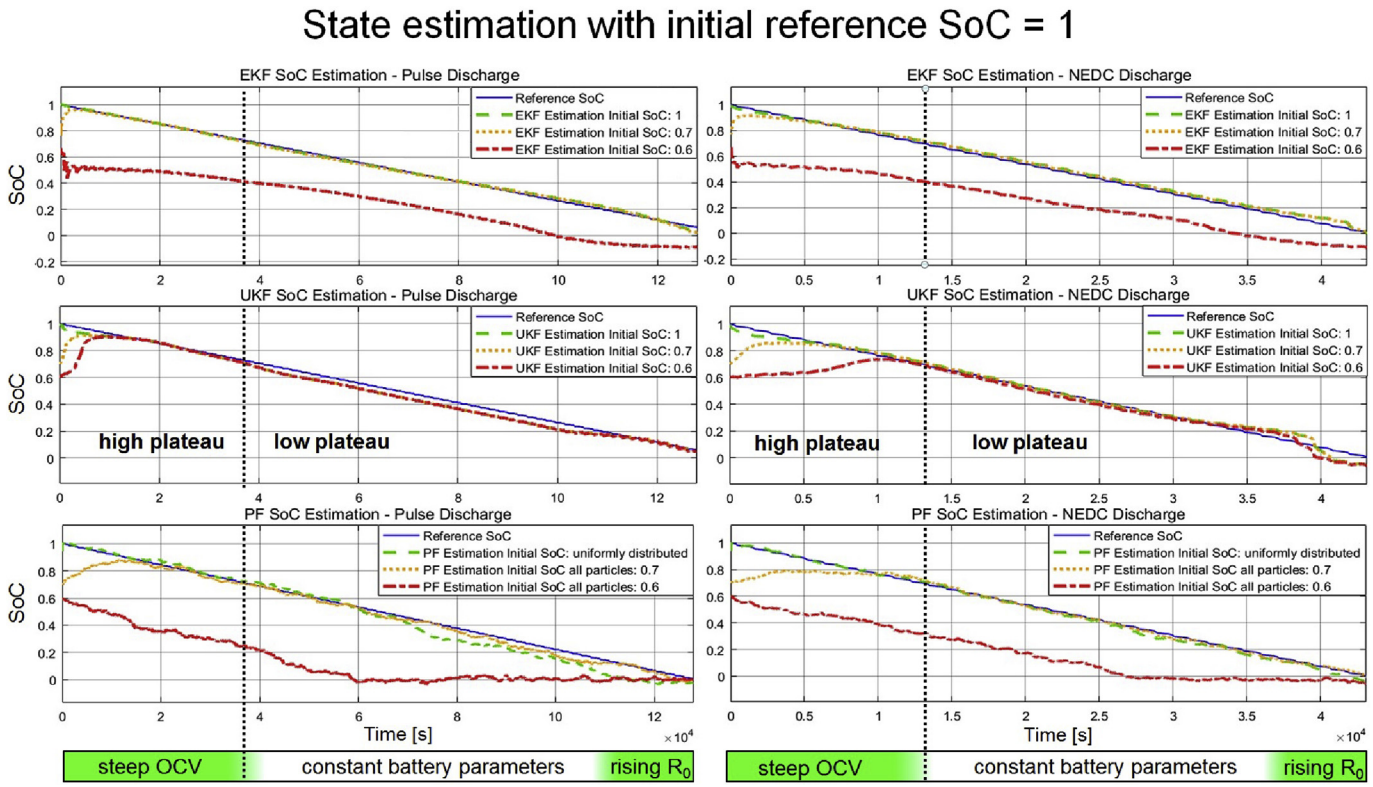

Fig. 4. Estimation results for EKF, UKF, PF with a mixed pulse- and a NEDC drive cycle current profile, starting with a fully charged battery, i.e. SoC = 1.

Table 2
RSME SoC Estimation with EKF, UKF and PF with initially fully charged battery.

Algorithm	SoC_0	Pulse RSME	NEDC RSME
EKF	1	0.0114	0.0217
	0.7	0.0160	0.0267
	0.6	0.2986	0.2732
UKF	1	0.0347	0.0280
	0.7	0.0444	0.0537
	0.6	0.0705	0.1199
PF	uni	0.0576	0.0195
	0.7	0.0532	0.0694
	0.6	0.3997	0.3354

Table 3
RSME SoC Estimation with EKF, UKF and PF with partly discharged battery.

Algorithm	SoC_0	Pulse RSME	NEDC RSME
EKF	1	0.1593	0.1696
	0.7	0.0860	0.0535
	0.6	0.1203	0.0745
UKF	1	0.0887	0.1743
	0.7	0.0240	0.0687
	0.6	0.0189	0.0332
PF	uni	0.0281	0.0561
	0.7	0.1661	0.1176
	0.6	0.0383	0.0320

the SoC estimators since the state changes when the monitoring system is switched off. However, the high plateau has also a steep OCV gradient which allows the estimator to converge quickly when the state changed. Therefore the estimation result does not change significantly with an imprecise initial condition as long as both states, the real one and the estimated one, are within the same plateau. Otherwise, the local minimum in the OCV can hinder the convergence. Especially the EKF, with its first order linearisation, and the PF with its particle set far away from the real SoC suffer from this effect (Fig. 4 EKF: Pulse Test, NEDC PF: Pulse Test, NEDC). Here, the UKF has the best performance. For applications demanding a quick conversion without a precise initial condition a self-discharge model is recommended.

Constant OCV: The uncertain region does not contain sufficient information in the battery behaviour to distinguish different SoCs in the low plateau, which leads to a state prediction heavily based on the Coulomb counting. The result of this is a slightly drifting SoC in that region and a slow convergence (Fig. 4 all filters: Pulse test, NEDC initial $SoC_{0\ \mathrm{ref}} = 1$). However, due to the area with increased internal resistance towards the end of discharge, the estimators are able to correct that error mostly before the depletion point. Here, the fact that the constant region is enclosed by the high plateau and an area of increased cell resistance favours the model based estimation. Furthermore, the lower self-discharge within the low plateau allows the Coulomb counting to be accurate and limits the drift.

Conversion with discharged battery: When starting from a partially-discharged state, e.g. where the self-discharge of the battery causes the estimated SoC to be higher than the real one (Fig. 5), the differences between the EKF and UKF are more pronounced. Here, the simulation was started at the initial reference SoC of 0.6, with the same initial conditions used in the fully-charged tests for the estimators ($SoC_{0EKF,UKF,PF} = 1, 0.7, 0.6$). In these tests, it can be seen that the estimators performance is also depending on the starting point. In general, the UKFs work best, though they can fail (Fig. 5 UKF NEDC initial $SoC_{0\ \mathrm{ref}} = 0.6$). The EKF tends to converge slowly, requiring more than a full discharge cycle. The particle filter can fail if the particles are poorly distributed at the start, but when the particles are uniformly distributed, it converges to the true state of charge very quickly. The results are summarized in Table 3.

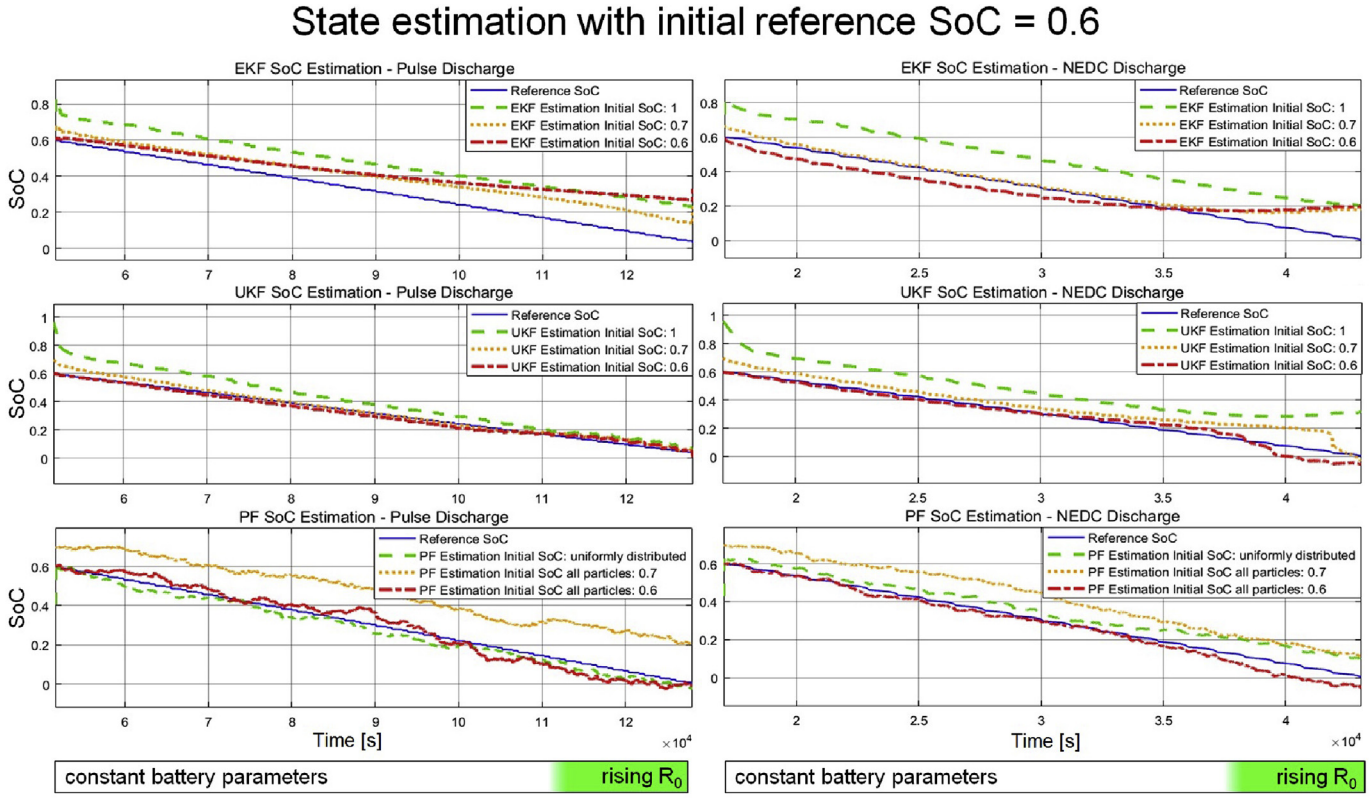

Fig. 5. Estimation results for EKF, UKF, PF with a mixed pulse- and a NEDC drive cycle current profile with an initially partly discharged battery, i.e. from SoC = 0.6.

Table 4
Discharge experiments with NEDC-low and NEDC-high profile.

Discharge	Measured Cap.	Av. Power	Av. Temp.
NEDC-low	10561 As	0.317 W	23 °C
NEDC-high	9072 As	0.610 W	23 °C

Changes of the model parameters: As mentioned before, the smaller parameter variation within the low plateau favours the SoC estimation. However, the dependence of the battery behaviour on the load profile remains a challenge. Different current rates and profiles cause different utilisations of sulfur and therefore variations in the usable capacity. While these effects are less pronounced in the high plateau, the low plateaus variations are significant. To show their effect to the model accuracy and SoC estimation, further tests were done with a decreased (added gain of 0.66 to current profile) and increased (added gain of 1.33 to current profile) NEDC profile (Table 4).

Both, Fig. 6 and Fig. 7, show the effects of the current density variations to the model accuracy and SoC estimation. For most of the discharge range the cell behaviour could still be represented well. But the increased capacity, mainly in the low plateau, leads to deviations of model prediction and measured voltage towards the end of discharge (Fig. 6), since the model uses the fixed capacity value from the pulse identification process (9778 As).

The rough capacity prediction combined with the constant OCV within the low plateau cause a negative drift of the SoC estimation in this area. Due to the strong divergence between model and measurements towards the end of discharge however, there is some correction towards the reference SoC in the end of the discharge process as well.

With higher rates the ratio of the high plateau of the whole discharge capacity increases which should enable the algorithms to correct the states longer. Nevertheless, the estimated SoC drifts towards higher values in this case. Here the differences in between the model and measurements are not significant enough to correct the states sufficiently. The results of the estimation accuracy with different current profile gains are summarized in Table 5.

To cover for the uncertainties, an improved observer model, accounting for model changes with current profiles, could be the key for improvement. However, since the inner cell mechanisms are still a matter of ongoing research, on-line parameter estimation could lead to improvements for the SoC estimation easier to obtain.

To achieve optimal results with handling the proposed model and estimation, we suggest the following steps: (i) define a simplified current profile for the intended application; (ii) measure the delivered capacities for this use-case and (iii) apply our presented battery model and estimation method with the derived capacity value.

Two plateaus with transition region: A likely consequence of the local minimum in the identified OCV curve in between the voltage plateaus, the EKF and the PF converge slowly when the initial condition is not located in the high plateau ($SoC_0 = 0.6$). To investigate filter-based solutions to improve the convergence, a simplified OCV curve, neglecting the voltage drop in between the plateaus (Fig. 8), was fitted to the OCV identification data and substituted with the previously used function.

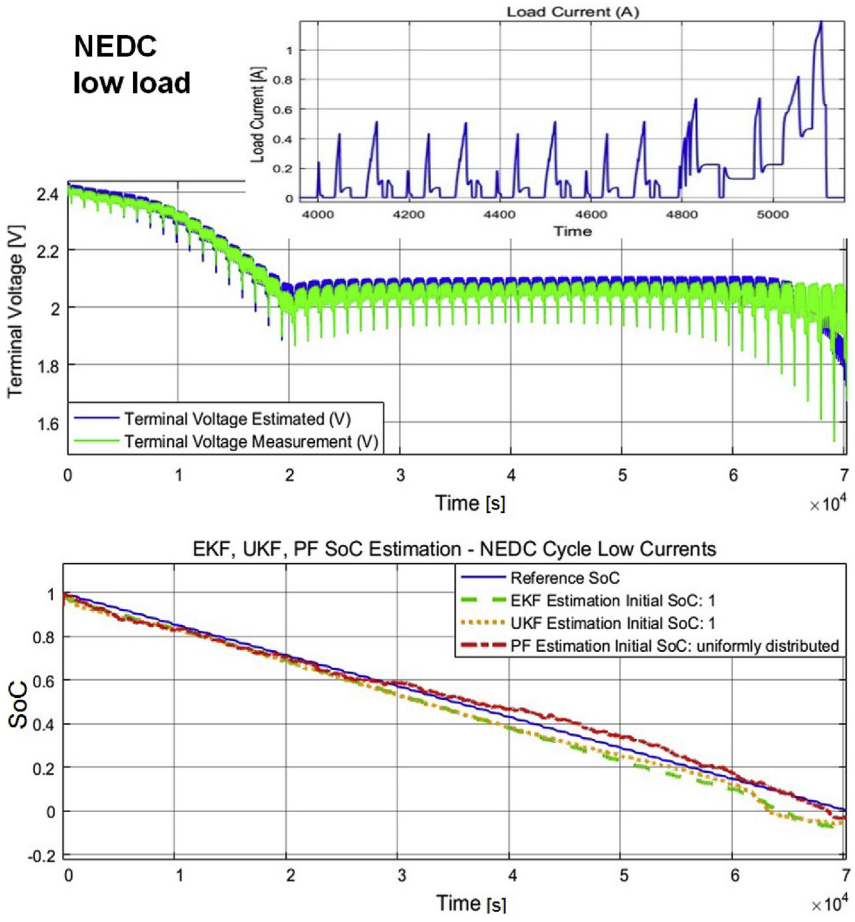

Fig. 6. Estimation results EKF, UKF, PF for a lower current NEDC drive cycle (Added gain of 0.66 to the reference NEDC drive cycle, described in Sec. 5).

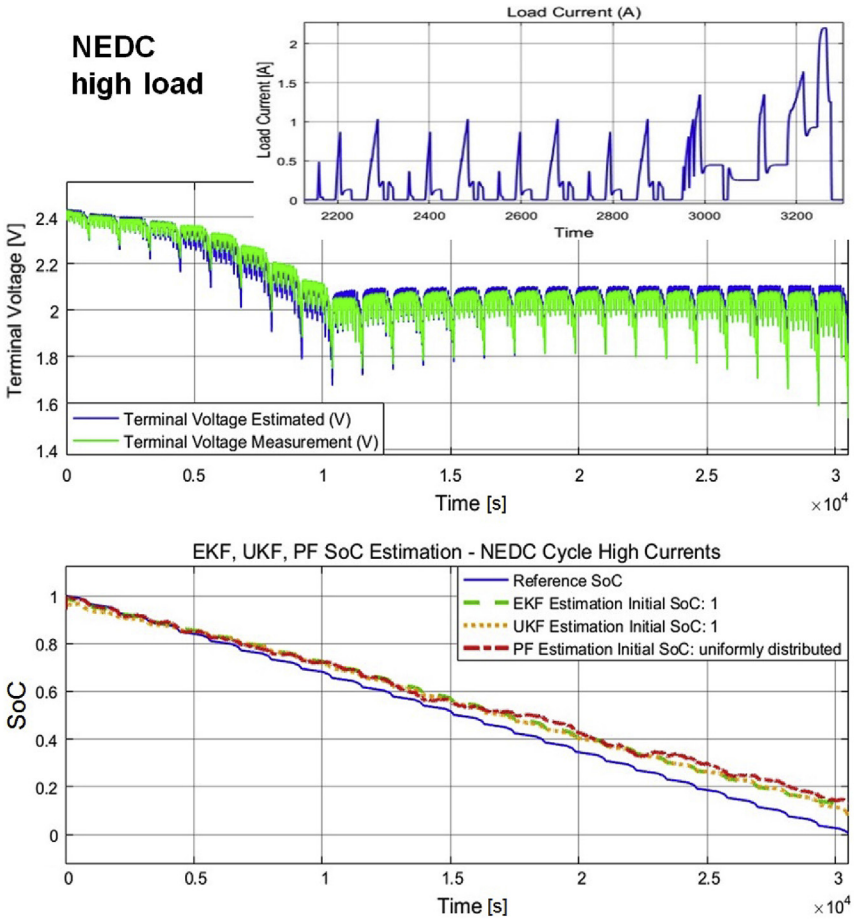

Fig. 7. Estimation results EKF, UKF, PF for a higher current NEDC drive cycle (Added gain of 1.33 to the reference NEDC drive cycle, described in Sec. 5).

Table 5
RSME SoC estimation with NEDC-low and NEDC-high profile.

Algorithm	SoC_0	NEDC-low	NEDC-high
EKF	1	0.0489	0.0580
UKF	1	0.0625	0.0546
PF	uni	0.0310	0.0694

$$f_{OCV-simple}(x_2) = 339.78x_2^9 - 1372.71x_2^8 + 2291.23x_2^7 - 2066.02x_2^6 + 1107.76x_2^5 - 364.76x_2^4 + 72.94x_2^3 - 8.36x_2^2 + 0.48x_2 + 2.1 \quad (26)$$

The advantage of this single polynomial is an almost monotonic behaviour ignoring highly nonlinear parts in the OCV curve, also simplifying the derivation of the Jacobian matrix. While the estimation results of the PF do not change significantly, the first order linearisation of the EKF leads to the anticipated results. As shown in Fig. 8, the convergence time for the imprecise initial SoC of 0.6 has improved significantly with only minor losses in the estimation accuracy for the rest of the discharge (Table 6).(For the simplified OCV curve, it was found necessary to set the initial covariance of the SoC to 21.)

However, all in all we can conclude that the UKF can cope best with the properties of the Li-S battery combined with a reasonable computational effort. Table 7 presents the simulation times for the reference battery model and three parallel running estimation algorithms (SoC_0: 1, 0.7, 0.6) on the same system (Intel(R) Core(TM) i5-5300 CPU @ 2.30 Ghz, 8GB RAM, 64 bit operating system).

It is shown that the additional computational effort of the particle filter does not lead to significant improvements in this case.

7. Conclusion

This paper has introduced the problem of SoC estimation for Li-S batteries, and explored the applicability of 'standard' techniques used for lithium-ion batteries. It was noted that Li-S batteries exhibit complex behaviours, some of which prevent the exploitation of 'standard' techniques in electric vehicles. Lithium-sulfur's open-circuit–voltage versus state-of-charge curve has a large flat region, meaning that open-circuit voltage is a poor indicator of SoC. Because there are multiple reaction pathways, the useful capacity of Li-S cells depends on the applied duty cycle. Furthermore, it suffers from high self-discharge, so 'Coulomb counting' is unlikely to be effective. As an alternative, this paper has explored three model-based methods of state estimation, all of which were variants of the recursive Bayesian filter: the extended Kalman filter, the unscented Kalman filter and the particle filter. Despite the complexities of Li-S cells, it was demonstrated in experimental tests that the model-based estimators based on an equivalent-circuit–network model were able to perform robustly.

The discussion of the results noted several ways where the complex behaviours of Li-S help to aid the estimation problem. While the high self-discharge within the high plateau hinders the determination of a precise initial SoC, the steep OCV gradient in this

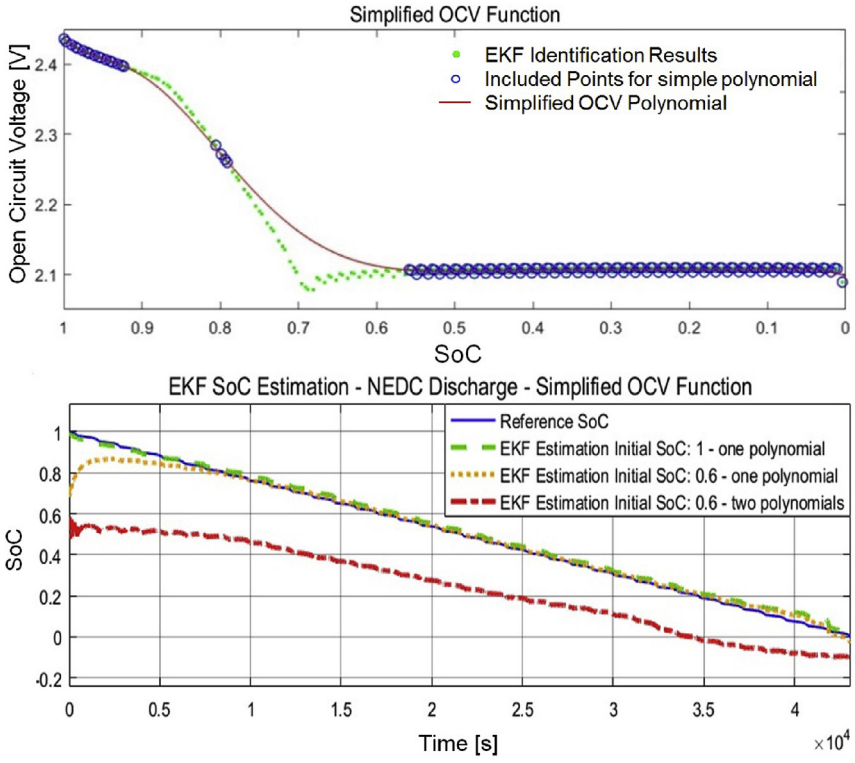

Fig. 8. Simplified OCV curve and related estimation results for the EKF.

Table 6
RSME SoC estimation with simplified OCV curve.

Algorithm	SoC_0	OCV Function	NEDC RSME
EKF	1	one poly	0.0205
	0.6	one poly	0.0272
	0.6	two poly	0.3923

Table 7
Simulation time for the pulse discharge test (128000 s).

	EKF	UKF	PF
Simulation time	5.25 [s]	7.97 [s]	21.54 [s]

region allows a quick convergence. Here, problematic and useful properties for the state estimation cancel each other out. In the low plateau, the flat OCV curve and relative constant battery parameters hinder a precise estimation. In this area also current-related changes in the usable capacity occur mostly, which is the reason why the proposed estimation methods works best within a certain discharge current range. However, due to the enclosure of the constant region by the high plateau and an area with increased internal resistance, the estimation is mostly able to converge to the correct SoC within one discharge cycle. Therefore a standard model-based estimator, with its multiple sources/states of information, is capable of predicting the SoC of a Li-S cell well enough. Hereby the unscented Kalman filter gives the most robust and accurate performance in combination with a reasonable computational effort.

It was conjectured that improvements to the model to represent self-discharge are likely to benefit the robustness of the estimators. Furthermore, a facility to deal with the current-related parameter changes, is very likely to improve the accuracy. It would also be interesting to consider whether adaptive noise covariance values could be used to improve the model fit whilst accommodating regions of greater uncertainty. The authors also are currently exploring the application of recursive parameter estimation for state estimation. A limitation of the performed tests is the constant-temperature scenario. This mirrors the highly regulated environment of the authors' intended end application, an electric vehicle test environment with a tightly-regulated temperature. However, future work should also explore any challenges associated with state estimation in an environment with significant temperature variations.

Acknowledgement

This research was undertaken as part of the project 'Revolutionary Electric Vehicle Battery' (REVB), co-funded by Innovate UK under grant TS/L000903/1; university funding is provided by EPSRC under grant number EP/L505286/1. Enquiries for access to the data referred to in this article should be directed to researchdata@cranfield.ac.uk. (The data used in this article is described at https://dx.doi.org/10.17862/cranfield.rd.3834057; it is subject to an embargo, and will be available from May 2022.)

References

[1] P.G. Bruce, S.A. Freunberger, L.J. Hardwick, J.-M. Tarascon, Li-o2 and li-s batteries with high energy storage, Nat. Mater. 11 (2012) 19–29.
[2] D. Bresser, S. Passerini, B. Scrosati, Recent progress and remaining challenges in sulfur-based lithium secondary batteries–a review, Chem. Commun. 49 (2013) 10545–10562.
[3] V. Kolosnitsyn, E. Karaseva, Lithium-sulfur batteries: problems and solutions, Russ. J. Electrochem. 44 (2008) 506–509.
[4] X. Ji, L.F. Nazar, Advances in li–s batteries, J. Mater. Chem. 20 (2010) 9821–9826.
[5] OXIS Engery Ltd, Lithium Sulfur Battery Technology, (accessed February 3, 2016). URL: http://www.oxisenergy.com.
[6] Sion Power Corporation, Sion Power Licerion Li-s Battery Li-Sulfur high-energy density lithium-sulfur rechargeable battery, (accessed April 18, 2016).

URL: http://www.sionpower.com.
[7] M.U. Cuma, T. Koroglu, A comprehensive review on estimation strategies used in hybrid and battery electric vehicles, Renew. Sustain. Energy Rev. 42 (2015) 517–531.
[8] A. Fotouhi, D.J. Auger, K. Propp, S. Longo, M. Wild, A review on electric vehicle battery modelling: from lithium-ion toward lithium–sulphur, Renew. Sustain. Energy Rev. 56 (2016) 1008–1021.
[9] V. Ramadesigan, P.W. Northrop, S. De, S. Santhanagopalan, R.D. Braatz, V.R. Subramanian, Modeling and simulation of lithium-ion batteries from a systems engineering perspective, J. Electrochem. Soc. 159 (2012) R31–R45.
[10] L. Lu, X. Han, J. Li, J. Hua, M. Ouyang, A review on the key issues for lithium-ion battery management in electric vehicles, J. Power Sources 226 (2013) 272–288.
[11] L.W. Yao, J. Aziz, P.Y. Kong, N. Idris, Modeling of lithium-ion battery using matlab/simulink, in: Industrial Electronics Society, IECON 2013-39th Annual Conference of the IEEE, IEEE, 2013, pp. 1729–1734.
[12] M. Chen, G.A. Rincon-Mora, Accurate electrical battery model capable of predicting runtime and iv performance, Energy Convers. IEEE Trans. 21 (2006) 504–511.
[13] O. Erdinc, B. Vural, M. Uzunoglu, A dynamic lithium-ion battery model considering the effects of temperature and capacity fading, in: Clean Electrical Power, 2009 International Conference on, IEEE, 2009, pp. 383–386.
[14] J. Xu, C.C. Mi, B. Cao, J. Deng, Z. Chen, S. Li, The state of charge estimation of lithium-ion batteries based on a proportional-integral observer, Veh. Technol. IEEE Trans. 63 (2014) 1614–1621.
[15] S. Piller, M. Perrin, A. Jossen, Methods for state-of-charge determination and their applications, J. Power Sources 96 (2001) 113–120.
[16] G.L. Plett, Sigma-point kalman filtering for battery management systems of lipb-based hev battery packs, J. Power Sources 161 (2006) 1356–1368.
[17] M. Wild, L. ONeill, T. Zhang, R. Purkayastha, G. Minton, M. Marinescu, O. GJ, Lithium sulfur batteries, a mechanistic review, Energy Environ. Sci. 8 (2015) 3477–3494.
[18] K. Propp, M. Marinescu, D.J. Auger, L. O'Neill, A. Fotouhi, K. Somasundaram, G.J. Offer, G. Minton, S. Longo, M. Wild, et al., Multi-temperature state-dependent equivalent circuit discharge model for lithium-sulfur batteries, J. Power Sources 328 (2016) 289–299.
[19] A. Manthiram, Y. Fu, S.-H. Chung, C. Zu, Y.-S. Su, Rechargeable lithium–sulfur batteries, Chem. Rev. 114 (2014) 11751–11787.
[20] H.S. Ryu, Z. Guo, H.J. Ahn, G.B. Cho, H. Liu, Investigation of discharge reaction mechanism of lithium— liquid electrolyte— sulfur battery, J. Power Sources 189 (2009) 1179–1183.
[21] M.U. Patel, R. Demir-Cakan, M. Morcrette, J.-M. Tarascon, M. Gaberscek, R. Dominko, Li-s battery analyzed by uv/vis in operando mode, ChemSusChem 6 (2013) 1177–1181.
[22] M. Marinescu, T. Zhang, G.J. Offer, A zero dimensional model of lithium–sulfur batteries during charge and discharge, Phys. Chem. Chem. Phys. 18 (2016) 584–593.
[23] H. Yamin, E. Peled, Electrochemistry of a nonaqueous lithium/sulfur cell, J. Power Sources 9 (1983) 281–287.
[24] Y.V. Mikhaylik, I. Kovalev, R. Schock, K. Kumaresan, J. Xu, J. Affinito, High energy rechargeable li-s cells for ev application: status, remaining problems and solutions, Ecs Trans. 25 (2010) 23–34.
[25] Y.V. Mikhaylik, J.R. Akridge, Polysulfide shuttle study in the li/s battery system, J. Electrochem. Soc. 151 (2004) A1969–A1976.
[26] Y. Diao, K. Xie, S. Xiong, X. Hong, Shuttle phenomenon–the irreversible oxidation mechanism of sulfur active material in li–s battery, J. Power Sources 235 (2013) 181–186.
[27] B. Pattipati, C. Sankavaram, K.R. Pattipati, System identification and estimation framework for pivotal automotive battery management system characteristics, Syst. Man Cybern. Part C Appl. Rev. IEEE Trans. 41 (2011) 869–884.
[28] K. Kutluay, Y. Cadirci, Y.S. Özkazanç, I. Cadirci, A new online state-of-charge estimation and monitoring system for sealed lead-acid batteries in telecommunication power supplies, Ind. Electron. IEEE Trans. 52 (2005) 1315–1327.
[29] V. Knap, D.-I. Stroe, M. Swierczynski, R. Teodorescu, E. Schaltz, Investigation of the self-discharge behavior of lithium-sulfur batteries, J. Electrochem. Soc. 163 (2016) A911–A916.
[30] M.R. Busche, P. Adelhelm, H. Sommer, H. Schneider, K. Leitner, J. Janek, Systematical electrochemical study on the parasitic shuttle-effect in lithium-sulfur-cells at different temperatures and different rates, J. Power Sources 259 (2014) 289–299.
[31] P. Singh, C. Fennie, D. Reisner, Fuzzy logic modelling of state-of-charge and available capacity of nickel/metal hydride batteries, J. Power Sources 136 (2004) 322–333.
[32] P. Singh, R. Vinjamuri, X. Wang, D. Reisner, Design and implementation of a fuzzy logic-based state-of-charge meter for li-ion batteries used in portable defibrillators, J. Power Sources 162 (2006) 829–836.
[33] A. Fotouhi, D.J. Auger, K. Propp, S. Longo, Electric vehicle battery parameter identification and soc observability analysis: Nimh and li-s case studies, in: 8th IET International Conference on Power Electronics, Machines and Drives (PEMD), 2016.
[34] A. Jossen, Fundamentals of battery dynamics, J. Power Sources 154 (2006) 530–538.
[35] H. He, R. Xiong, H. Guo, S. Li, Comparison study on the battery models used for the energy management of batteries in electric vehicles, Energy Convers. Manag. 64 (2012) 113–121.
[36] J. Li, J.K. Barillas, C. Guenther, M.A. Danzer, A comparative study of state of charge estimation algorithms for lifepo 4 batteries used in electric vehicles, J. Power Sources 230 (2013) 244–250.
[37] Z. Chen, Y. Fu, C.C. Mi, State of charge estimation of lithium-ion batteries in electric drive vehicles using extended kalman filtering, Veh. Technol. IEEE Trans. 62 (2013) 1020–1030.
[38] D. Yang, G. Qi, X. Li, State-of-charge estimation of lifepo 4/c battery based on extended kalman filter, in: Power and Energy Engineering Conference (APPEEC), 2013 IEEE PES Asia-Pacific, IEEE, 2013, pp. 1–5.
[39] Y. Tian, B. Xia, W. Sun, Z. Xu, W. Zheng, A modified model based state of charge estimation of power lithium-ion batteries using unscented kalman filter, J. Power Sources 270 (2014) 619–626.
[40] F. Sun, X. Hu, Y. Zou, S. Li, Adaptive unscented kalman filtering for state of charge estimation of a lithium-ion battery for electric vehicles, Energy 36 (2011) 3531–3540.
[41] W. He, N. Williard, C. Chen, M. Pecht, State of charge estimation for electric vehicle batteries using unscented kalman filtering, Microelectron. Reliab. 53 (2013) 840–847.
[42] L. Zhong, C. Zhang, Y. He, Z. Chen, A method for the estimation of the battery pack state of charge based on in-pack cells uniformity analysis, Appl. Energy 113 (2014) 558–564.
[43] X. Liu, Z. Chen, C. Zhang, J. Wu, A novel temperature-compensated model for power li-ion batteries with dual-particle-filter state of charge estimation, Appl. Energy 123 (2014) 263–272.
[44] S. Schwunk, N. Armbruster, S. Straub, J. Kehl, M. Vetter, Particle filter for state of charge and state of health estimation for lithium–iron phosphate batteries, J. Power Sources 239 (2013) 705–710.
[45] S. Thrun, W. Burgard, D. Fox, Probabilistic Robotics, MIT Press, 2005.
[46] R. Karlsson, Particle Filtering for Positioning and Tracking Applications, Linköping University Electronic Press, 2005.
[47] G. Welch, G. Bishop, An Introduction to the Kalman Filter, Department of Computer Science, University of North Carolina, 2006.
[48] D. Simon, Kalman filtering, Embed. Syst. Program. 14 (2001) 72–79.
[49] MATLAB Version 8.5.0.197613 (R2015a), The Mathworks, Inc., Natick, Massachusetts, 2015.
[50] G.L. Plett, Extended kalman filtering for battery management systems of lipb-based hev battery packs, J. Power Sources 134 (2004) 252–261.
[51] M. Rhudy, Y. Gu, Understanding nonlinear kalman filters, part ii: an implementation guide, Interact. Robot. Lett. (2013).
[52] M.S. Arulampalam, S. Maskell, N. Gordon, T. Clapp, A tutorial on particle filters for online nonlinear/non-gaussian bayesian tracking, Signal Process. IEEE Trans. 50 (2002) 174–188.
[53] A. Papazoglou, S. Longo, D. Auger, F. Assadian, Computational aspects of estimation algorithms for battery-management systems, in: 8th Conference on Sustainable Development of Energy, Water and Enviroment Systems, 2013.
[54] S. Thrun, W. Burgard, D. Fox, Probabilistic Robotics, Intelligent Robotics and Autonomous Agents, MIT Press, Cambridge and Mass, 2005.
[55] S. Samuel, L. Austin, D. Morrey, Automotive test drive cycles for emission measurement and real-world emission levels-a review, in: Proceedings of the Institution of Mechanical Engineers, Part D: Journal of Automobile Engineering vol. 216, 2002, pp. 555–564.
[56] R. Kötz, S. Müller, M. Bärtschi, B. Schnyder, P. Dietrich, F. Büchi, A. Tsukada, G. Scherer, P. Rodatz, O. Garcia, et al., Supercapacitors for peak-power demand in fuel-cell-driven cars, in: ECS Electro-chemical Society, 52nd Meeting, San Francisco, 2001.